PAPER

Projectile transverse momentum controls emission in electron vortex ionization collisions

To cite this article: A Plumadore and A L Harris 2020 J. Phys. B: At. Mol. Opt. Phys. 53 205205

View the article online for updates and enhancements.



IOP ebooks™

Bringing together innovative digital publishing with leading authors from the global scientific community.

Start exploring the collection-download the first chapter of every title for free.

Projectile transverse momentum controls emission in electron vortex ionization collisions

A Plumadore and A L Harris * 10

Physics Department, Illinois State University, Normal, IL, 61790, United States of America

E-mail: alharri@ilstu.edu

Received 26 May 2020, revised 11 August 2020 Accepted for publication 28 August 2020 Published 25 September 2020



Abstract

The realization of electron vortex (EV) beams in the past decade has led to numerous proposed applications in fields from electron microscopy to control and manipulation of individual molecules. Yet despite the many unique characteristics and promising advantages of EV beams, such as transverse momentum and quantized orbital angular momentum, there remains a limited understanding of their fundamental interactions with matter at the atomic scale. Collisions between EV projectiles and atomic targets can provide some insight into these interactions and we present here fully differential cross sections (FDCS) for ionization of excited state atomic hydrogen targets using EV projectiles. We show that the projectile's transverse momentum causes the ionized electron angular distributions to be altered compared to non-vortex projectiles and that the ionized electron's ejection angle can be controlled by adjustment of the vortex opening angle, a feature unique to vortex projectiles. Additionally, an inherent uncertainty in the projectile's momentum transfer leads to a broadening of the classical binary peak, making signatures of the target electron density more readily observable. FDCS for aligned 2p targets exhibit structures can be used to determine the alignment.

Keywords: ionization, electron vortex beam, momentum transfer

(Some figures may appear in colour only in the online journal)

1. Introduction

For many decades, fundamental discoveries about the structure of atoms and molecules have been made through the field of charged particle collisions [1]. These studies have provided an invaluable amount of information about electron charge cloud distributions and Coulomb interactions in few-body systems. Despite their long history, atomic collisions are still providing new insights, and even surprises, thanks to improved theoretical methods and advanced experimental technologies. In recent years, the COLTRIMS experimental technique has driven advancements by providing unprecedented detailed measurements [2]. Complementary to this, many theoretical models such as exterior complex scaling [3], convergent close coupling [4], time dependent close coupling [5], and *R*-matrix with pseudostates [6] models are now

considered numerically exact for some collision processes, essentially solving the three-body problem. Looking ahead, electron vortex (EV) beams may provide the next leap forward in atomic and molecular collisions, providing a new probe of atomic structure and charged particle dynamics.

EV beams are matter waves with non-zero orbital angular momentum and transverse linear momentum. They have recently been experimentally realized by several groups [7–11], and may provide the opportunity for control and rotation of nanoparticles [12–15], improved resolution in electron microscopy [12, 16, 17], as well as the study of fundamental atomic properties, such as the magnetic moment and electronic transitions [12, 13, 18]. The development of EV beams was inspired by their optical counterparts, which have been widely studied [19] and are used extensively in applications such as optical tweezers [20, 21], microscopy [22, 23], micromanipulation [24] and astronomy [25]. EV beams, however, provide

^{*} Author to whom any correspondence should be addressed.

advantages their photonic counterparts cannot, such as smaller wavelengths that allow for more precise interactions with small molecules [26]. EV beams also inherently carry charge, leading to electric and magnetic effects that can be exploited to improve microscopy applications [7].

While *optical* vortex beams have a long history of study and successful application, the study and application of EV beams is still in its infancy. The proposed applications of EV beams are far-reaching and development of these applications requires a solid understanding of their interactions at the atomic scale, with atomic collision cross sections providing a vital piece of the puzzle. In addition, EV beams present a new tool for atomic and molecular collision physics itself to more intimately explore the fundamental interactions and structures of the particles in these collisions.

In [27, 28], we showed that the fully differential cross sections (FDCS) for ionization of ground state hydrogen using EV projectiles were significantly altered compared to their non-vortex counterparts. We present here theoretical FDCS for ionization of atomic hydrogen from the first two excited states by EV projectiles. The present results show clear signatures of the target state structure that are not visible in the FDCS of non-vortex projectiles. We also show that FDCS for EV projectiles with carefully chosen physical characteristics can be used to identify the orientation of a spatially asymmetric target. These results are an analogue and initial test case for future studies aimed at identifying molecular structure and orientation. Through kinematical arguments, we explain the qualitative structures observed in the FDCS and show how these features can be traced to characteristics of either the target atom or vortex projectile. Atomic units are used throughout.

2. Theory

EV beams are experimentally generated using high energy electrons on the order of a few keV, making the first Born approximation (FBA) sufficient for the calculation of FDCS. Details of the FBA model for ionization by EV projectile can be found in [27, 28], and we present only the essential information here. The FDCS for ionization by EV projectile is

$$\frac{\mathrm{d}^3 \sigma}{\mathrm{d}\Omega_1 \mathrm{d}\Omega_2 \mathrm{d}E_2} = \mu_{\mathrm{pa}}^2 \mu_{\mathrm{ie}} \frac{k_f k_e}{k_i} \left| T_{\mathrm{fi}}^V(\vec{q}) \right|^2, \tag{1}$$

where $T_{fi}^V(\vec{q})$ is the transition matrix element and the momenta of the incident projectile, scattered projectile, and ionized electron are $\vec{k}_i, \vec{k}_f, \vec{k}_e$ respectively. The momentum transfer vector is given by $\vec{q} = \vec{k}_i - \vec{k}_f$, and the reduced masses of the projectile and target atom and the proton and ionized electron are $\mu_{\rm pa}$ and $\mu_{\rm je}$, respectively.

The vortex transition matrix element is given by

$$T_{\rm fi}^V = -(2\pi)^{3/2} \left\langle \Psi_{\rm f} \left| V_i \right| \Psi_{\rm i} \right\rangle, \tag{2}$$

where $\Psi_{i,f}$ is the initial (final) state wave function and V_i is the perturbation, which is simply the Coulomb interaction between the projectile and target atom

$$V_i = -\frac{1}{r_1} + \frac{1}{r_{12}}. (3)$$

The projectile-nuclear distance is r_1 and the projectile-target electron distance is r_{12} .

The initial state wave function is a product of the incident projectile Bessel wave function $\chi_{\vec{k}_i}(\vec{r}_1)$ and the target hydrogen atom wave function $\Phi(\vec{r}_2)$

$$\Psi_{i} = \chi_{\vec{k}} (\vec{r}_{1}) \Phi (\vec{r}_{2}). \tag{4}$$

The target hydrogen atom wave function is known analytically and readily available in any quantum mechanics textbook. The Bessel wave function can also be written analytically and although similar to the more familiar plane wave function, has some key differences. Like the plane wave function, the Bessel wave function has infinite extent in the transverse direction. However, unlike the plane wave, the Bessel wave function has quantized orbital angular momentum, and as a result, is not uniform in the transverse direction. Instead, it has a phase singularity at a specific spatial location. To define the location of the phase singularity, we define the z-axis to be along the longitudinal incident projectile momentum direction with the target atom located at the origin. Then, an impact parameter b can be defined that describes the transverse location of the phase singularity relative to the z-axis. For an impact parameter of $|\vec{b}| = 0$, the Bessel wave function is a free particle solution to the Schrödinger equation in cylindrical coordinates (ρ_1, φ_1, z_1) , and can be written as

$$\chi_{\vec{k}_i}(\vec{r}_1) = \frac{e^{il\varphi_1}}{2\pi} J_l(k_{i\perp}\rho_1) e^{ik_{iz}z_1}$$
 (5)

where $k_{i\perp}$ and k_{iz} are the vortex projectile's transverse and longitudinal momenta and l is the quantized orbital angular momentum. These linear momenta can be written in terms of the beam's opening angle α as

$$k_{i\perp} = k_i \sin \alpha,$$
 (6)

and

$$k_{iz} = k_i \cos \alpha. \tag{7}$$

From equations (5) and (6), it is clear that, unlike the plane wave, the Bessel wave function has non-zero transverse momentum. In fact, one of the inherent features of a vortex projectile is that the transverse momentum is not well-defined; only the magnitude of the transverse momentum is specified, not its azimuthal angle. This uncertainty in incident momentum can also be seen by writing the Bessel wave function as a superposition of tilted plane waves [29]

$$\chi_{\vec{k}_i}(\vec{r}_1) = \frac{(-i)^l}{(2\pi)^2} \int_0^{2\pi} d\phi_{ki} \ e^{il\phi_{ki}} \ e^{i\vec{k}_i \cdot (\vec{r}_1 - \vec{b})}, \tag{8}$$

where ϕ_{ki} is the azimuthal angle of the incident projectile momentum. As discussed below, this leads to an uncertainty in the momentum transfer vector, which has a noticeable effect on the FDCS.

The final state wave function is a product of the scattered projectile plane wave $\chi_{\vec{k}_f}(\vec{r}_1)$ and the ionized electron wave function $\chi_{\vec{k}_a}(\vec{r}_2)$

$$\Psi_f = \chi_{\vec{k}_f}(\vec{r}_1) \chi_{\vec{k}_e}(\vec{r}_2). \tag{9}$$

No post-collision interaction between the two outgoing electrons in the final state is included because only highly asymmetric energy sharing is studied here, making the effects of the post-collision interaction negligible. The plane wave for the scattered projectile is given by

$$\chi_{\vec{k}_f}(\vec{r}_1) = \frac{e^{i\vec{k}_f \cdot \vec{r}_1}}{(2\pi)^{3/2}}.$$
 (10)

For the kinematics considered here, the ionized electron is much slower than the projectile, and we have improved upon the model in [27, 28] by now representing the ionized electron by a Coulomb wave in the field of the residual H^+ ion

$$\chi_{\vec{k}_e}(\vec{r}_2) = \Gamma (1 - i\eta) e^{-\frac{\pi\eta}{2}} \frac{e^{i\vec{k}_e \cdot \vec{r}_2}}{(2\pi)^{3/2}} {}_1F_1 \left(i\eta, 1, -ik_e r_2 - i\vec{k}_e \cdot \vec{r}_2 \right),$$
(11)

where $\Gamma(1-i\eta)$ is the gamma function and η is the Sommer-feld parameter.

Combining the above equations yields the following integral form for the vortex transition matrix in terms of the plane wave transition matrix $T_{fi}^{\text{PW}}(\vec{q}\,)$

$$T_{fi}^{V}(\vec{q}) = \frac{(-i)^{l}}{(2\pi)} \int_{0}^{2\pi} d\phi_{ki} e^{il\phi_{ki}} T_{fi}^{PW}(\vec{q}) e^{-i\vec{k}_{i} \cdot \vec{b}}, \qquad (12)$$

where $T_{fi}^{\rm PW}(\vec{q})$ is calculated for incident $\chi_{\vec{k}_i}$ and scattered $\chi_{\vec{k}_f}$ projectile plane waves

$$T_{fi}^{\text{PW}} = \frac{-1}{(2\pi)} \int d\vec{r}_1 d\vec{r}_2 \ e^{i\vec{q}\cdot\vec{r}_1} \chi_{\vec{k}_e}^*(\vec{r}_2) V_i \Phi(\vec{r}_2). \tag{13}$$

Equation (12) is the transition matrix for ionization by an incident Bessel projectile with fixed impact parameter. However, in an experiment, it is not possible to control the impact parameter for each collision event, and therefore an average over impact parameters is necessary. As detailed in [27, 28, 30], the FDCS averaged over impact parameter is equivalent to an average over incident momentum azimuthal angles and can be conveniently written in terms of the non-vortex plane wave transition matrix

$$\frac{\mathrm{d}^3 \sigma}{\mathrm{d}\Omega_1 \mathrm{d}\Omega_2 \mathrm{d}E_2} = \mu_{\mathrm{pa}}^2 \mu_{pi} \frac{k_f k_e}{(2\pi) k_{zi}} \int \mathrm{d}\phi_{k_i} \left| T_{fi}^{\mathrm{PW}} \left(\vec{q} \right) \right|^2. \tag{14}$$

In order to calculate the FDCS using equation (14), one needs to write the momentum transfer vector \vec{q} in terms of its components, including the vortex opening angle and projectile momentum azimuthal angle. In the collision system used here, the final state projectile scatters into the x-z plane with scattering angle θ_s and positive x-coordinate. By definition, the x-z plane is the scattering plane and contains the incident longitudinal momentum and scattered projectile momentum vector, but not necessarily the momentum transfer vector. Because the incident momentum vector can have a non-zero y-component

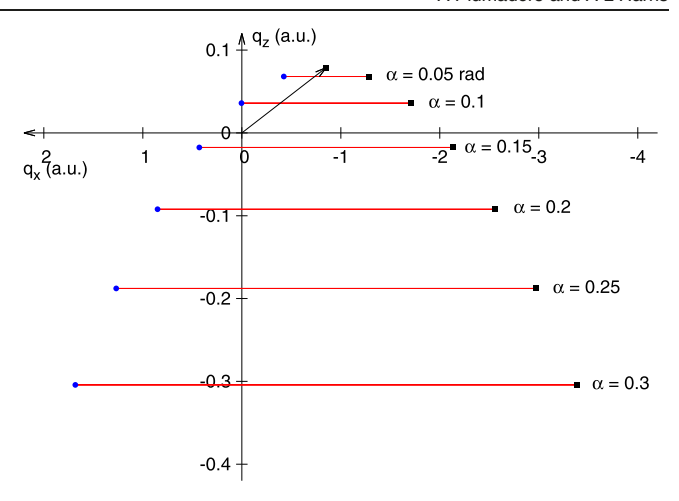


Figure 1. Momentum transfer vector projections in the scattering plane for an EV projectile for all possible ϕ_{ki} . Each opening angle α has a set of momentum transfer vectors that lie on a cone. The heads of these vectors appear as a line (red) when projected onto the scattering plane. For an incident plane wave, there is only one momentum transfer vector (black arrow). The blue circles at the minimum q_x values occur for $\phi_{ki} = 0$ and the black squares at the maximum q_x values occur for $\phi_{ki} = \pi$. Results are shown for an incident projectile energy of 1 keV, scattering angle 100 mrad, ionized electron energy 5 eV, and n = 2 hydrogen target.

that lies outside the scattering plane, the momentum transfer vector is also not restricted to lie in the scattering plane. In this coordinate system, the momentum transfer vector components are given by

$$q_x = k_i \sin \alpha \cos \phi_{k_i} - k_f \sin \theta_{\rm s} \tag{15}$$

$$q_{y} = k_{i} \sin \alpha \sin \phi_{k_{i}} \tag{16}$$

$$q_z = k_i \cos \alpha - k_f \cos \theta_s, \tag{17}$$

where θ_s is the projectile scattering angle. Because the incident momentum is uncertain, with only the magnitude of transverse momentum specified, the momentum transfer \vec{q} is also uncertain. This uncertainty in the momentum transfer is accounted for by averaging the FDCS over the incident momentum azimuthal angle (see equation (14)).

For each azimuthal angle ϕ_{k_i} , there is a unique momentum transfer vector, which has its tail at the origin. The set of vortex momentum transfer vectors then form a cone with the point at the origin. If the heads of the vectors forming the cone are projected onto the scattering plane, they lie along a line parallel to the x-axis. In other words, for a given opening angle, the longitudinal components of the vortex momentum transfer vectors are constant. Figure 1 shows a plot of the projection of the heads of the momentum transfer vectors in the scattering plane as a function of ϕ_{ki} for several opening angles. For a nonvortex projectile, there is only a single, well-defined momentum transfer vector shown in figure 1 as a solid black arrow. We refer to this as the classical momentum transfer. If $\phi_{k_i} = 0$ or π , the vortex momentum transfer vector lies in the scattering plane, while for all other values of ϕ_{k_i} , the momentum transfer vector points outside the scattering plane. As the opening angle increases, the spread of the vortex momentum transfer vectors increases, resulting in larger uncertainty in the momentum transfer vector. Additionally, for an opening angle greater than the scattering angle, some of the vortex momentum transfer vectors have a transverse component in the same direction as the scattered projectile (positive *x*-component). We show below that this has a significant effect on the ejected electron angular distributions. These features of momentum transfer uncertainty hold for all excited states of the target atom.

3. Results

For FDCS with EV projectiles averaged over impact parameter, the only physical parameter distinguishing the EV projectile from that of a plane wave is the opening angle α , which determines the projectile's transverse momentum. If $\alpha = 0$, the plane wave projectile is recovered and the incident projectile has only longitudinal momentum. For $\alpha \neq 0$, the incident vortex projectile has both longitudinal and transverse momentum $k_{i\perp}$, leading to the uncertainty in momentum transfer discussed above. This uncertainty has the effect of broadening the main peak in the FDCS as observed in figures 2 and 3, which show the FDCS for ionization of hydrogen from the ground and first two excited states as a function of ejected electron angle and opening angle. In figure 2, the FDCS are plotted as a heat map with the magnitude of the FDCS represented by color. A horizontal trace through the plots in figure 2 results in the FDCS for a fixed opening angle. A few select traces for $\alpha = 0, 0.05, 0.1$, and 0.15 rad are shown in figure 3. The kinematics were chosen such that future experiments may be possible (high incident energy) and the FBA is applicable (asymmetric outgoing electron energies and small perturbation parameter). For these FDCS, a 1 keV incident electron scatters from the target at a fixed scattering angle of 100 mrad (5.73°); the ionized electron has an energy of 5 eV. We note that the FDCS for other kinematical parameters exhibit the same qualitative behaviors observed here, and we begin with a discussion of some qualitative features present for all target states.

Figures 2 and 3 show that for small values of $\alpha \leq 0.05$ rad), the traditional binary peak due to a direct collision between the projectile and target electron is observed along the classical momentum transfer direction ($\theta_e = 81.8^{\circ}$ for n = 1, $\theta_{\rm e}=84.7^{\circ}$ for n=2, and $\theta_{\rm e}=85.3^{\circ}$ for n=3). However, no recoil peak along the direction opposite the classical momentum transfer direction is present due to the kinematics. As is well-understood in plane wave collisions, if the momentum transfer \vec{q} and initial target electron momentum are welldefined, then the binary peak would be sharp. However, the momentum distribution of the initial target electron results in a broad binary peak centered about the classical momentum transfer direction. The same broad binary peak is also observed for vortex collisions, however as the vortex opening angle α increases, the binary peak broadens even more due to the uncertainty in the momentum transfer. The location of the binary peak also shifts to smaller angles as opening angle increases.

For $\alpha > 0.1$ rad, the dominant peak is observed at the classical recoil peak direction, opposite to the classical momentum transfer direction. This shift is a result of one momentum transfer direction being dominant in the average over azimuthal angles. Because each non-vortex FDCS used in the average depends inversely on powers of the momentum transfer magnitude, FDCS from azimuthal angles resulting in smaller momentum transfer magnitude will dominate the average. Figure 4 shows the magnitude of the momentum transfer as a function of opening angle for all projectile momentum azimuthal angles. From this, it is clear that for a given opening angle, the smallest value of momentum transfer magnitude occurs for $\phi_{ki} = 0$ and the largest for $\phi_{ki} = \pi$. This indicates that the non-vortex FDCS for $\phi_{ki} \approx 0$ dominates the average, with the contributions of all other FDCS diminishing rapidly as ϕ_{ki} moves away from 0. Because $\phi_{ki} = 0$ is dominant in the average of the FDCS, the direction of the momentum transfer for this particular azimuthal angle is the primary influence of the peak location in the FDCS. It can be seen from figure 1 that the momentum transfer direction for $\phi_{k_i} = 0$ (blue circles) shifts to a more forward direction as α increases toward 0.1 rad, is exactly forward $(q_x = 0)$ at $\alpha = 0.1$ rad, and then is oriented backward for $\alpha > 0.1$ rad, which nicely correlates with the FDCS peak location.

A plot of the momentum transfer angle for $\phi_{ki} = 0$ compared to the peak location of the FDCS is shown in figure 5 for the ground state, where it is readily observable that the FDCS peak is almost exactly predicted by the momentum transfer direction for $\phi_{k_i} = 0$. Similar results are found for all but the 2pz excited state, which exhibits a double peak structure centered around the classical momentum transfer direction for $\phi_{k_i} = 0$. This explains the transition from a dominant peak along the classical binary peak direction to along the classical recoil peak direction, as seen in figures 2 and 3. In fact, this 'recoil' peak is actually the binary peak caused by a momentum transfer vector resulting from the projectile being deflected toward the beam direction (-x direction) rather than away from it (+x direction). This is a feature only possible with EV projectiles, as a non-vortex projectile is always deflected toward the +x direction for FDCS with fixed scattering angle and the geometry defined here. The shift in location of the binary peak provides a possible means to control ionized electron emission angle for fixed energies and scattering angle, which could have potential applications in electron microscopy or collisions with delicate targets. In these cases, low energy electrons may cause additional noise in a signal or possible damage to a target or sample. If the secondary electron could be primarily emitted into a region not of interest, the signal to noise ratio may be enhanced or the lifetime or survivability of the sample improved.

The FDCS for $\alpha=0.1$ rad exhibit features that are significantly different than those for other opening angles. This is because for $\alpha=\theta_s$ and $\phi_{k_i}=0$, the incident projectile has approximately the same transverse momentum as the scattered projectile, resulting in only longitudinal momentum transferred to the target. Purely longitudinal momentum transfer then results in two peaks in the FDCS parallel (0°) and

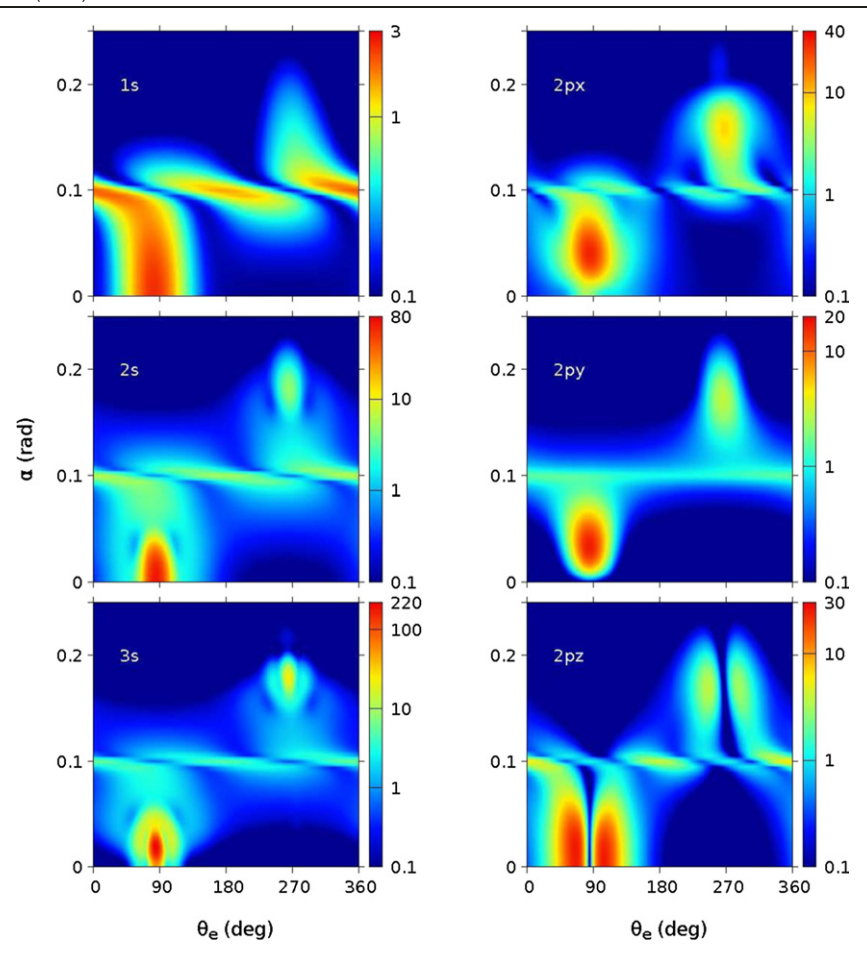


Figure 2. FDCS for ionization of H by EV projectile as a function of EV opening angle α (vertical axis) and ionized electron angle θ_e (horizontal axis). The color bar represents the magnitude of the FDCS in atomic units. The incident projectile energy is 1 keV, scattering angle is 100 mrad, and ionized electron energy is 5 eV. The target state is shown in the figure.

antiparallel (180°) to the beam direction for spherically symmetric target s-states. The FDCS for spatially oriented target p-states exhibit different features for $\alpha=\theta_s$ due to their initial state orientations. Details of these features are discussed below.

Also, for the excited s-state targets, interference structures can be observed in the FDCS due to the multilobe structure of the target. While present for most values of α , including $\alpha=0$ non-vortex projectiles, the interference patterns are most noticeable for α near θ_s . This is likely due to the spreading of the dominant lobe as the uncertainty in the momentum transfer increases, making the interference structures more visible. For non-vortex projectiles, the interference structures are one to three orders of magnitude below the dominant binary peak, making them difficult to observe. However, for vortex projectiles, the interference structures are within an order of magnitude of the maximum of the FDCS, and therefore more easily visible.

Unlike the s-state targets, the 2p target is not spherically symmetric and can serve as an analogue for diatomic molecule targets, where nuclear alignment effects are known to be important [31, 32]. As seen from figures 2 and 3, the orientation of the target in the 2p state has a significant influence on the shape of the FDCS, although some of the

features observed in the s-state FDCS persist. For $\alpha < \theta_s$, the FDCS for 2pz orientation show a minimum along the classical momentum transfer direction with equal magnitude peaks on either side of this direction. This is because the 2pz plane wave transition matrix is minimized for the ejected electron momentum along the momentum transfer direction. For 2py orientation, the FDCS are zero at $\alpha=0$ due to zero target wave function density in the scattering plane and the momentum transfer vector lying in the scattering plane. However, the use of a vortex projectile results in an out-of-plane component to the momentum transfer, which can then produce electrons ejected into the scattering plane, resulting in a single binary peak in the FDCS. A similar binary peak structure is seen in the 2px FDCS, which is enhanced for vortex projectiles.

One of the most interesting features of the 2p FDCS is the structure observed with $\alpha=\theta_s$. As for the s-states, the $\phi_{k_i}=0$ FDCS is dominant and the primary momentum transfer direction is parallel to the beam direction. Therefore, any structures observed at ionized electron angles other than 0° or 180° must be due to the target electron's initial momentum or spatial distribution. For 2px orientation, two peaks in the FDCS are observed to either side of the classical beam direction, possibly caused by the target electron being offset to either

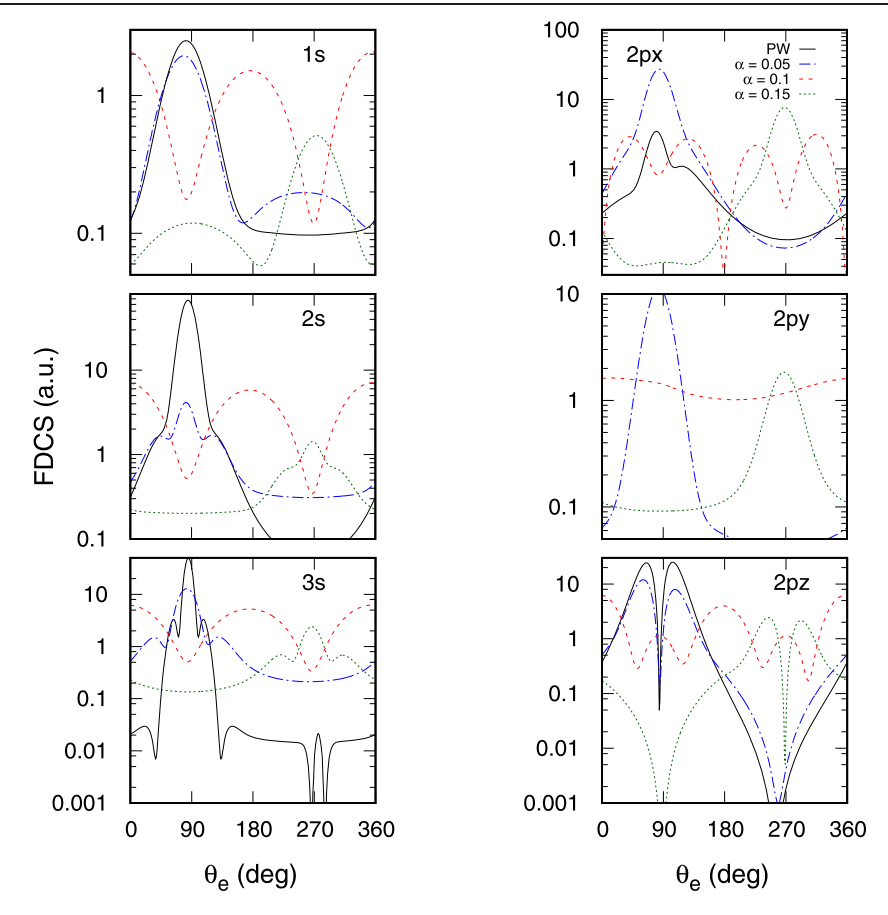


Figure 3. Fixed opening angle FDCS from horizontal traces through the plots of figure 2.

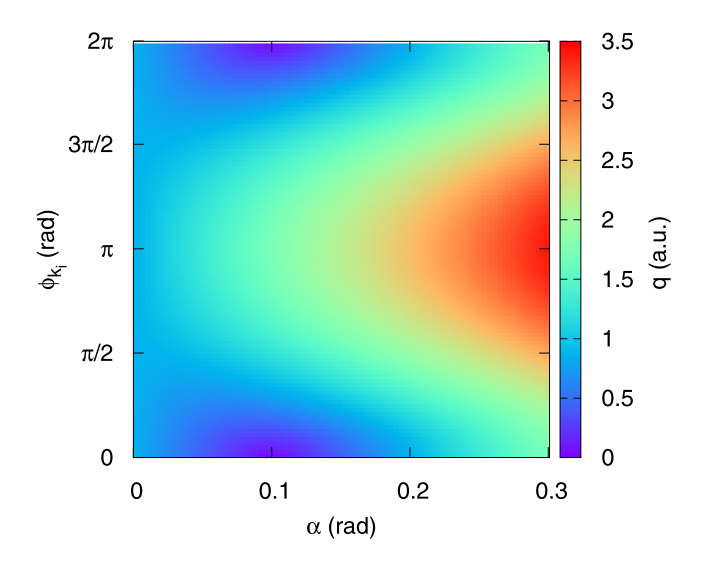


Figure 4. Magnitude of momentum transfer as a function of projectile opening angle α and incident momentum azimuthal angle ϕ_{k_i} . The incident projectile energy is 1 keV, scattering angle 100 mrad, ionized electron energy 5 eV, and n=2 hydrogen target.

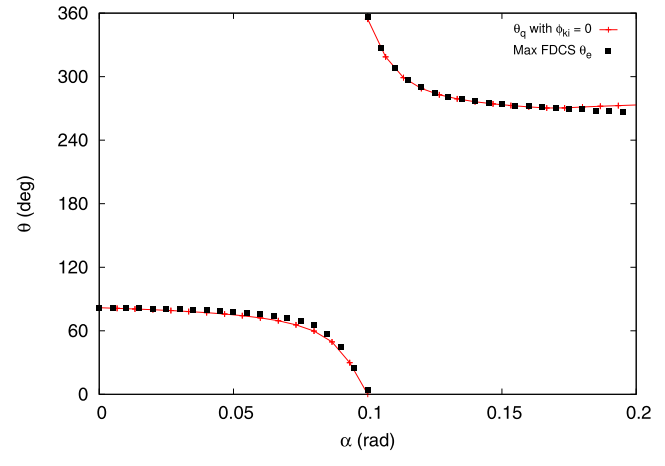


Figure 5. Momentum transfer angle (red line) as measured counterclockwise from the beam direction for incident momentum with azimuthal angle $\phi_{k_i}=0$. Also shown is the ionized electron angle (black squares) corresponding to the maximum FDCS value. The incident projectile energy is 1 keV, scattering angle 100 mrad, ionized electron energy 5 eV, and ground state hydrogen target.

side of the beam direction with zero density along the *z*-axis. This initial spatial distribution, combined with a momentum transfer vector along the beam direction, then results in an ionized electron distribution primarily located to either side of

the beam direction. For 2py orientation, the ionized electrons are nearly uniformly distributed due to the initial state electron distribution being symmetric about the scattering plane with zero initial state density in the scattering plane. For

2pz orientation, peaks are observed along and opposite the beam direction due to the momentum transfer along the beam direction and the electron density oriented along the beam direction. The strong dependence of the FDCS on 2p target orientation, along with the easily observable interference structures in the 2s and 3s FDCS provide preliminary evidence that the target orbital structure and orientation can be deduced from the FDCS using EV projectiles. This is a promising indicator that EV collisions may be used to characterize molecular structure.

4. Conclusion

FDCS for ionization of atomic hydrogen excited states by EV projectiles show signatures of atomic orbital structure and target orientation. Some of these features are not present in FDCS for non-vortex projectiles and others are more enhanced when EV projectiles are used. In particular, clear signatures of orientation effects were seen in the FDCS for 2p targets, and interference effects were observed for 2s and 3s targets resulting from their nodal structure. Analysis of the FDCS revealed that while the momentum of the incident projectile, and therefore the momentum transfer, is uncertain, the FDCS are dominated by an incident projectile with azimuthal angle $\phi_{k_i} = 0$. As the opening angle of the EV projectile is varied, the uncertainty in the momentum transfer leads to a spreading of the ejected electron binary peak. The location of the binary peak was strongly correlated with the momentum transfer direction for an incident projectile with $\phi_{k_i} = 0$.

The results here demonstrate the potential feasibility of using ionization cross sections to infer target structure information, a requirement for some of the proposed applications of EV projectiles, such as characterization of chiral molecule enantiomers [13]. Our results also demonstrate a possible mechanism for controlling ionized electron emission angle by altering the EV opening angle. The FDCS presented here provide valuable fundamental information for use in potential applications of EV projectile collisions and provide proof of principle that EV projectiles yield information not available or easily accessible by non-vortex projectiles.

Acknowledgments

We gratefully acknowledge the support of the NSF under Grant No. PHY-1912093.

ORCID iDs

A L Harris https://orcid.org/0000-0003-2689-982X

References

- [1] Bransden B H and Joachain C J 2003 *Physics of Atoms and Molecules* 2nd edn (Englewood Cliffs, NJ: Prentice-Hall)
- [2] Dörner R, Mergel V, Jagutzki O, Spielberger L, Ullrich J, Moshammer R and Schmidt-Böcking H 2000 Phys. Rep. 330 95
- [3] Rescigno T N, Baertschy M, Isaacs W A and McCurdy C W 1999 Science 286 2474
- [4] Bray I 2002 Phys. Rev. Lett. 89 273201
- [5] Colgan J and Pindzola M S 2006 Phys. Rev. A 74 012713
- [6] Bartschat K and Bray I 1996 Phys. Rev. A 54 R1002
- [7] Verbeeck J, Tian H and Schattschneider P 2010 Nature 467 301
- [8] Uchida M and Tonomura A 2010 Nature 464 737
- [9] McMorran B J, Agrawal A, Anderson I M, Herzing A A, Lezec H J, McClelland J J and Unguris J 2011 Science 331 192
- [10] Grillo V, Gazzadi G C, Mafakheri E, Frabboni S, Karimi E and Boyd R W 2015 Phys. Rev. Lett. 114 034801
- [11] Voloch-Bloch N, Lereah Y, Lilach Y, Gover A and Arie A 2013 Nature 494 331
- [12] Schattschneider P, Schaffer B, Ennen I and Verbeeck J 2012 Phys. Rev. B 85 134422
- [13] Asenjo-Garcia A and García de Abajo F J 2014 Phys. Rev. Lett. 113 066102
- [14] Babiker M, Bennett C R, Andrews D L and Dávila Romero L C 2002 Phys. Rev. Lett. 89 143601
- [15] Verbeeck J, Tian H and Van Tendeloo G 2013 Adv. Mater. 25 1114
- [16] Rusz J and Bhowmick S 2013 Phys. Rev. Lett. 111 105504
- [17] Lloyd S, Babiker M and Yuan J 2012 Phys. Rev. Lett. 108 074802
- [18] Bhattacharya M, Haimberger C and Bigelow N P 2003 Phys. Rev. Lett. 91 213004
- [19] Nye J F and Berry M V 1974 Proc. R. Soc. A 336 165
- [20] He H, Friese M E J, Heckenberg N R and Rubinsztein-Dunlop H 1995 Phys. Rev. Lett. 75 826
- [21] O'Neil A T, MacVicar I, Allen L and Padgett M J 2002 Phys. Rev. Lett. 88 053601
- [22] Fürhapter S, Jesacher A, Bernet S and Ritsch-Marte M 2005 Opt. Express 13 689
- [23] Baranek M and Bouchal Z 2013 J. Eur. Opt. Soc. 8 13017
- [24] Galajda P and Ormos P 2001 Appl. Phys. Lett. 78 249
- [25] Berkhout G C G and Beijersbergen M W 2009 J. Opt. A: Pure Appl. Opt. 11 094021
- [26] Lloyd S M, Babiker M, Thirunavukkarasu G and Yuan J 2017 Rev. Mod. Phys. 89 035004
- [27] Harris A L, Plumadore A and Smozhanyk Z 2019 J. Phys. B: At. Mol. Opt. Phys. 52 094001
- [28] Harris A L, Plumadore A and Smozhanyk Z 2020 J. Phys. B: At. Mol. Opt. Phys. 53 109501
- [29] Van Boxem R, Partoens B and Verbeeck J 2015 Phys. Rev. A 91 032703
- [30] Serbo V, Ivanov I P, Fritzsche S, Seipt D and Surzhykov A 2015 Phys. Rev. A 92 012705
- [31] Colgan J, Pindzola M S, Robicheaux F, Kaiser C, Murray A J and Madison D H 2008 Phys. Rev. Lett. 101 233201
- [32] Li X, Ren X, Hossen K, Wang E, Chen X and Dorn A 2018 Phys. Rev. A 97 022706